Critical Behaviour of the Ferromagnetic Spin-$\frac{3}{2}$ Blume-Emery-Griffiths Model with Repulsive Biquadratic Coupling

M. Ali Pınar[a], Mustafa Keskin[b], Ahmet Erdinç[b], and Osman Canko[b]

[a] Institute of Science, Erciyes University, 38039 Kayseri, Turkey
[b] Department of Physics, Erciyes University, 38039 Kayseri, Turkey

Reprint requests to Prof. M. K.; E-mail: keskin@erciyes.edu.tr

Z. Naturforsch. **62a,** 127 – 139 (2007); received January 31, 2007

The critical behaviour of the ferromagnetic spin-$\frac{3}{2}$ Blume-Emery-Griffiths model with repulsive biquadratic coupling in the absence and presence of an external magnetic field is studied by using the lowest approximation of the cluster variation method, which is identical with the mean-field approximation. Thermal variations of the order parameters are investigated for different values of the interaction parameters and the external magnetic field. The complete phase diagrams of the system are calculated in the $(kT/J,K/J)$, $(kT/J,D/J)$ and $(kT/J,H/J)$ planes. Five new phase diagram topologies are obtained, which are either absent from previous approaches or have gone unnoticed. A detailed discussion and comparison of the phase diagrams is made.

Key words: Spin-$\frac{3}{2}$ Blume-Emery-Griffiths Model; Cluster Variation Method; Thermal Variations of Order Parameters; Phase Diagrams.

1. Introduction

The spin-$\frac{3}{2}$ Ising model Hamiltonian with bilinear (J) and biquadratic (K) nearest-neighbour pair interactions and a single-ion potential or crystal-field interaction (D) is known as the spin-$\frac{3}{2}$ Blume-Emery-Griffiths (BEG) model and is probably the simplest extension of the spin-1 BEG model, which presents a rich variety of critical and multicritical phenomena. The spin-$\frac{3}{2}$ BEG model is defined by the Hamiltonian

$$H = -J\sum_{\langle ij\rangle} S_i S_j - K\sum_{\langle ij\rangle} {S^2}_i {S^2}_j + D(\sum_i {S^2}_i), \quad (1)$$

where each S_i can take the values $\pm 3/2$ and $\pm 1/2$ and $\langle ij\rangle$ indicates summation over all pairs of nearest-neighbour sites.

The spin-$\frac{3}{2}$ BEG model, with J and K interactions, was initially introduced [1] in connection with experimental results on magnetic and crystallographic phase transitions in some rare-earth compounds such as $DyVO_4$ [2], and its phase diagram was determined within the mean-field approximation (MFA). A modified version of the spin-$\frac{3}{2}$ Ising model was later introduced [3] to describe tricritical properties in ternary fluid mixtures and was also solved within the MFA. The results were compared with experimental observations on the system ethanol/water/carbon dioxide. The spin-$\frac{3}{2}$ BEG model is the most general spin-$\frac{3}{2}$ Ising model. The spin-$\frac{3}{2}$ Ising model Hamiltonian with only J and D interactions is known the spin-$\frac{3}{2}$ Blume-Capel (BC) model and the spin-$\frac{3}{2}$ Ising model Hamiltonian with only J and K interactions is known as isotropic spin-$\frac{3}{2}$ BEG model.

The critical properties of the ferromagnetic spin-$\frac{3}{2}$ BEG model for $K/J > 0$ have been studied, and its phase diagrams have been presented by a variety of methods, such as renormalization-group (RG) methods [4], the effective field theory (EFT) [5], the Monte Carlo (MC) simulations and a density-matrix RG method [6]. An exact formulation of the model on a Bethe lattice was studied by using the exact recursion equations [7].

On the other hand, the ferromagnetic spin-$\frac{3}{2}$ BEG model with repulsive biquadratic coupling, i. e. $K/J < 0$ has also been studied. An early attempt to study the spin-$\frac{3}{2}$ BEG model with $K/J < 0$ was made by Sâ Barretto and De Alcamtara Bonfim [8], and Bakkali et al. [9] within the MFA and also the MC calculation, and the EFT, respectively. Sâ Barretto and De Alcamtara Bonfim [8] calculated only the phase diagrams for the ferromagnetic isotropic spin-$\frac{3}{2}$ BEG model and Bakkali et al. [9] also presented two phase diagrams: one for the ferromagnetic spin-$\frac{3}{2}$ BC model and the other for the ferromagnetic isotropic

spin-$\frac{3}{2}$ BEG model. Tucker [10] studied the ferromagnetic spin-$\frac{3}{2}$ BEG model with $K/J < 0$ by using the cluster variation method in pair approximation (CVMPA) and only presented the phase diagrams of the spin-$\frac{3}{2}$ BC model and isotropic spin-$\frac{3}{2}$ BEG model for several values of the coordination number. Backhich and El Bouziani [11] calculated the phase diagram of the model in the $(kT/J,D/J)$ plane for only the two different values of K/J within an approximate renormalization-group approach of the Migdal-Kadanoff type. Hence, in these studies [9–11], only some portions of the global phase diagrams of the ferromagnetic spin-$\frac{3}{2}$ BEG model in a zero external magnetic field have been considered. Recently, Ekiz et al. [12] investigated the ferromagnetic spin-$\frac{3}{2}$ BEG model in a Bethe lattice using the exact recursion equations and presented the phase diagrams in the $(kT/J,K/J)$ plane for several values of D/J and in the $(kT/J,D/J)$ plane for several values of K/J in the absence of an external magnetic field, H. Ekiz [13] extended the previous work for the presence of an external magnetic field [12]. He presented one phase diagram in the $(kT/J,H/J)$ plane and for $K/J=-0.5$ and $D/J=1.0$ and one phase diagram in the $(kT/J,K/J)$ plane for $H/J=2.0$ and $D/J=0.5$ for the coordination numbers $q=3$, 4, 6 and 8.

The purpose of the present paper is to study the temperature dependence of order parameters of the two-sublattice ferromagnetic spin-$\frac{3}{2}$ BEG model for different values of interaction parameters and an external magnetic field, to calculate the global phase diagrams of the spin-$\frac{3}{2}$ BEG model in the absence and presence of the external magnetic field in detail, and to compare the results with the approximate methods [8–11] and the exact results on the Bethe lattice [12, 13]. These calculations have been carried out by using the lowest approximation of the cluster variation method (LACVM) [14], which is identical with the MFA. Our recent works [15–17] display that the LACVM, in spite of its simplicity and limitations such as the correlations of spin fluctuations have not been considered, is an adequate starting point in which, within this theoretical framework, it is easy to determine the complete phase diagrams. It also predicts the existence of multicritical points and it gives phase diagrams, that were obtained by exact and more sophisticated methods.

Finally, we should also mention that recently many researches have investigated the antiferromagnetic spin-$\frac{3}{2}$ BC [15] and spin-$\frac{3}{2}$ BEG [16] models and found very rich phase diagram topologies. Moreover, random spin-$\frac{3}{2}$ antiferromagnetic Heisenberg chains [18] and the random quantum antiferromagnetic spin-$\frac{3}{2}$ chain [19] have been studied using the RG calculations.

The remainder of this work is organized as follows. In Section 2, we define the model briefly and obtain its solutions at equilibrium within the LACVM. Thermal variations of the order parameters are investigated in Section 3. In Section 4, transition temperatures are calculated precisely, and the phase diagrams are presented in the $(kT/J,K/J)$, $(kT/J,D/J)$ and $(kT/J,H/J)$ planes. Section 5 contains the summary and discussion.

2. Model and Method

The spin-$\frac{3}{2}$ BEG model is defined as a two-sublattice model with spin variables $S_i=\pm\frac{3}{2}, \pm\frac{1}{2}$ and $S_j=\pm\frac{3}{2}, \pm\frac{1}{2}$ on sites of sublattices A and B, respectively. The average value of each of the spin states or states probability will be denoted by X_1^{A}, X_2^{A}, X_3^{A} and X_4^{A} on the sites of sublattice A and X_1^{B}, X_2^{B}, X_3^{B} and X_4^{B} on the sites of sublattice B, which are also called internal or the state or point variables. X_1^{A}, X_1^{B}; X_2^{A}, X_2^{B}; X_3^{A}, X_3^{B}; X_4^{A}, X_4^{B} are the fractions of the spin values $+\frac{3}{2}$, $+\frac{1}{2}$, $-\frac{1}{2}$ and $-\frac{3}{2}$ on A, B sublattices, respectively. These variables obey the following two normalization relations for A and B sublattices:

$$\sum_{i=1}^{4} X_i^{\mathrm{A}} = 1 \text{ and } \sum_{j=1}^{4} X_j^{\mathrm{B}} = 1. \tag{2}$$

In order to account for the possible two-sublattice structure we need six long-range order parameters, which are introduced as follows: $M_{\mathrm{A}} \equiv \langle S_i^{\mathrm{A}} \rangle$, $Q_{\mathrm{A}} \equiv \langle (S_i^{\mathrm{A}})^2 \rangle$, $R_{\mathrm{A}} \equiv \langle (S_i^{\mathrm{A}})^3 \rangle$, $M_{\mathrm{B}} \equiv \langle S_j^{\mathrm{B}} \rangle$, $Q_{\mathrm{B}} \equiv \langle (S_j^{\mathrm{B}})^2 \rangle$, $R_{\mathrm{B}} \equiv \langle (S_j^{\mathrm{B}})^3 \rangle$, for A and B lattices, respectively. $\langle \ldots \rangle$ denotes the thermal average M_{A} and M_{B} are the average magnetizations which are the excess of one orientation over the other orientation, called magnetizations. Q_{A} and Q_{B} are the quadrupolar moments which are the average squared magnetizations, and R_{A} and R_{B} are the octupolar order parameters for A and B sublattices, respectively.

The sublattice order parameters can be expressed in terms of the internal variables and are given by

$$M_{\mathrm{A}} \equiv \langle S_i^{\mathrm{A}} \rangle = \frac{3}{2}(X_1^{\mathrm{A}} - X_4^{\mathrm{A}}) + \frac{1}{2}(X_2^{\mathrm{A}} - X_3^{\mathrm{A}}),$$

$$M_{\mathrm{B}} \equiv \langle S_j^{\mathrm{B}} \rangle = \frac{3}{2}(X_1^{\mathrm{B}} - X_4^{\mathrm{B}}) + \frac{1}{2}(X_2^{\mathrm{B}} - X_3^{\mathrm{B}}),$$

$$
\begin{aligned}
Q_{\mathrm{A}} &\equiv \langle (S_i^{\mathrm{A}})^2 \rangle = \frac{9}{4}X_1^{\mathrm{A}} + \frac{1}{4}X_2^{\mathrm{A}} + \frac{1}{4}X_3^{\mathrm{A}} + \frac{9}{4}X_4^{\mathrm{A}}, \\
Q_{\mathrm{B}} &\equiv \langle (S_j^{\mathrm{B}})^2 \rangle = \frac{9}{4}X_1^{\mathrm{B}} + \frac{1}{4}X_2^{\mathrm{B}} + \frac{1}{4}X_3^{\mathrm{B}} + \frac{9}{4}X_4^{\mathrm{B}}, \\
R_{\mathrm{A}} &\equiv \langle (S_i^{\mathrm{A}})^3 \rangle = \frac{27}{8}(X_1^{\mathrm{A}} - X_4^{\mathrm{A}}) + \frac{1}{8}(X_2^{\mathrm{A}} - X_3^{\mathrm{A}}), \\
R_{\mathrm{B}} &\equiv \langle (S_j^{\mathrm{B}})^3 \rangle = \frac{27}{8}(X_1^{\mathrm{B}} - X_4^{\mathrm{B}}) + \frac{1}{8}(X_2^{\mathrm{B}} - X_3^{\mathrm{B}}). \quad (3)
\end{aligned}
$$

Using (2) and (3), the internal variables can be expressed as linear combinations of the order parameters:

$$
\begin{aligned}
X_1^{\mathrm{A}} &= \frac{1}{4}\left(Q_{\mathrm{A}} - \frac{1}{4}\right) + \frac{1}{6}\left(R_{\mathrm{A}} - \frac{M_{\mathrm{A}}}{4}\right), \\
X_1^{\mathrm{B}} &= \frac{1}{4}\left(Q_{\mathrm{B}} - \frac{1}{4}\right) + \frac{1}{6}\left(R_{\mathrm{B}} - \frac{M_{\mathrm{B}}}{4}\right), \\
X_2^{\mathrm{A}} &= \frac{1}{4}\left(\frac{9}{4} - Q_{\mathrm{A}}\right) + \frac{1}{2}\left(\frac{9}{4}M_{\mathrm{A}} - R_{\mathrm{A}}\right), \\
X_2^{\mathrm{B}} &= \frac{1}{4}\left(\frac{9}{4} - Q_{\mathrm{B}}\right) + \frac{1}{2}\left(\frac{9}{4}M_{\mathrm{B}} - R_{\mathrm{B}}\right), \\
X_3^{\mathrm{A}} &= \frac{1}{4}\left(\frac{9}{4} - Q_{\mathrm{A}}\right) + \frac{1}{2}\left(R_{\mathrm{A}} - \frac{9}{4}M_{\mathrm{A}}\right), \\
X_3^{\mathrm{B}} &= \frac{1}{4}\left(\frac{9}{4} - Q_{\mathrm{B}}\right) + \frac{1}{2}\left(R_{\mathrm{B}} - \frac{9}{4}M_{\mathrm{B}}\right), \\
X_4^{\mathrm{A}} &= \frac{1}{4}\left(Q_{\mathrm{A}} - \frac{1}{4}\right) + \frac{1}{6}\left(\frac{1}{4}M_{\mathrm{A}} - R_{\mathrm{A}}\right), \\
X_4^{\mathrm{B}} &= \frac{1}{4}\left(Q_{\mathrm{B}} - \frac{1}{4}\right) + \frac{1}{6}\left(\frac{1}{4}M_{\mathrm{B}} - R_{\mathrm{B}}\right).
\end{aligned} \quad (4)
$$

The Hamiltonian of such a two-lattice ferromagnetic spin-$\frac{3}{2}$ BEG model in an external magnetic field is

$$
\begin{aligned}
\mathcal{H} = &-J\sum_{\langle ij\rangle} S_i S_j - K\sum_{\langle ij\rangle} S_i^2 S_j^2 \\
&+ D\left(\sum_i S_i^2 + \sum_j S_j^2\right) - H\left(\sum_i S_i + \sum_j S_j\right),
\end{aligned} \quad (5)
$$

where J, K, D and H describe the bilinear interaction, biquadratic interaction, the single-ion anisotropy and an effect of an external magnetic field, respectively. The Hamiltonian and phase diagrams are invariant under the transformation $H \to -H$ and $S \to -S$. The bilinear and biquadratic interactions are restricted to the z nearest neighbour pair of spin, which is absorbed in J and K.

The equilibrium properties of the system are determined by the LACVM [14], which is identical to the MFA. The method consists of the following three steps: (i) consider a collection of weakly interacting systems and define the internal variables; (ii) obtain the weight factor in terms of the internal variables; and (iii) find the free energy expression and minimize it with respect to internal variables.

The weight factors W^{A} and W^{B}, which are the number of ways the internal variables can be arranged over the sites, can be expressed in terms of the internal variables for the A and B sublattices, respectively, as

$$
W^{\mathrm{A}} = \frac{N^{\mathrm{A}}!}{\prod_{i=1}^{4}(X_i^{\mathrm{A}}N^{\mathrm{A}})!} \text{ and } W^{\mathrm{B}} = \frac{N^{\mathrm{B}}!}{\prod_{j=1}^{4}(X_j^{\mathrm{B}}N^{\mathrm{B}})!}, \quad (6)
$$

where N^{A} and N^{B} are the number of lattice points on the A and B sublattices, respectively. On the other hand, a simple expression for the internal energy of the system is found by working out (5) in the LACVM. This leads to

$$
\begin{aligned}
\frac{E}{N} = &-JM_{\mathrm{A}}M_{\mathrm{B}} - KQ_{\mathrm{A}}Q_{\mathrm{B}} \\
&+ D(Q_{\mathrm{A}} + Q_{\mathrm{B}}) - H(M_{\mathrm{A}} + M_{\mathrm{B}}),
\end{aligned} \quad (7)
$$

where N ($N = N^{\mathrm{A}} + N^{\mathrm{B}}$) is the number of total lattice points. Substituting (3) into (7), the internal energy per site can be written as

$$
\begin{aligned}
\frac{E}{N} = &-J\left[\frac{3}{2}(X_1^{\mathrm{A}} - X_4^{\mathrm{A}}) + \frac{1}{2}(X_2^{\mathrm{A}} - X_3^{\mathrm{A}})\right]\left[\frac{3}{2}(X_1^{\mathrm{B}} - X_4^{\mathrm{B}}) + \frac{1}{2}(X_2^{\mathrm{B}} - X_3^{\mathrm{B}})\right] \\
&- K\left[\frac{9}{4}(X_1^{\mathrm{A}} + X_4^{\mathrm{A}}) + \frac{1}{4}(X_2^{\mathrm{A}} + X_3^{\mathrm{A}})\right]\left[\frac{9}{4}(X_1^{\mathrm{B}} + X_4^{\mathrm{B}}) + \frac{1}{4}(X_2^{\mathrm{B}} + X_3^{\mathrm{B}})\right] \\
&+ D\left[\frac{9}{4}(X_1^{\mathrm{A}} + X_4^{\mathrm{A}}) + \frac{1}{4}(X_2^{\mathrm{A}} + X_3^{\mathrm{A}}) + \frac{9}{4}(X_1^{\mathrm{B}} + X_4^{\mathrm{B}}) + \frac{1}{4}(X_2^{\mathrm{B}} + X_3^{\mathrm{B}})\right] \\
&- H\left[\frac{3}{2}(X_1^{\mathrm{A}} - X_4^{\mathrm{A}}) + \frac{1}{2}(X_2^{\mathrm{A}} - X_3^{\mathrm{A}}) + \frac{3}{2}(X_1^{\mathrm{B}} - X_4^{\mathrm{B}}) + \frac{1}{2}(X_2^{\mathrm{B}} - X_3^{\mathrm{B}})\right].
\end{aligned} \quad (8)
$$

Fig. 1. Thermal variations of the sublattice order parameters, M_{A}, M_{B}, Q_{A} and Q_{B}. T_{C} and T_{t} are the second- and first-order phase transition temperatures for the sublattice order parameters. T_{CM} and T_{CQ} represent the critical or the second-order phase transition temperatures for only the sublattice magnetization and quadrupolar order parameters, respectively. (a) Two second-order phase transitions, one from the $\mathrm{f}_{3/2}$ phase to d phase for $K/J = 0.25$ and $D/J = 0.5$ (thick solid lines) and the other one from the $\mathrm{f}_{1/2}$ phase to d phase for $K/J = -0.5$ and $D/J = 0.5$ (thin solid lines). (b) First-order phase transition from the $\mathrm{f}_{3/2}$ phase to the d phase. $K/J = 1.25$ and $D/J = 1.5$. (c) Two successive phase transitions in which the first one is a first-order phase transition from the $\mathrm{f}_{3/2}$ phase to the $\mathrm{f}_{1/2}$ phase and the second one is a second-order phase transition from the $\mathrm{f}_{1/2}$ phase to the d phase. $K/J = -0.01$ and $D/J = 0.5$. (d) Two successive second-order phase transitions in which the first one is from the i phase to the a phase and the second one is from the a phase to the d phase. $K/J = -2.0$ and $D/J = -2.5$. (e) Three successive second-order phase transitions. The first one is from the $\mathrm{f}_{1/2}$ phase to the i phase, the second one is from the i phase to the $\mathrm{f}_{1/2}$ phase and the third is from the $\mathrm{f}_{1/2}$ phase to the d phase. The first two second-order transitions imply that the system exhibits a reentrant behaviour. $K/J = -1.0$ and $D/J = 0.05$. $\longrightarrow$

Using the definition of the entropy S ($S = k \ln W$, k is the Boltzmann factor) and making use of the Stirling approximation, the free energy f ($F = E - TS$) per site can be written as

$$f = \frac{F}{N} = -JM_{\mathrm{A}}M_{\mathrm{B}} - KQ_{\mathrm{A}}Q_{\mathrm{B}} + D(Q_{\mathrm{A}} + Q_{\mathrm{B}}) - H(M_{\mathrm{A}} + M_{\mathrm{B}}) + \frac{1}{\beta}\left\{\sum_{i=1}^{4} X_i^{\mathrm{A}} \ln X_i^{\mathrm{A}} + \sum_{j=1}^{4} X_j^{\mathrm{B}} \ln X_j^{\mathrm{B}}\right\} + \beta\lambda^{\mathrm{A}}\left\{1 - \sum_{i=1}^{4} X_i^{\mathrm{A}}\right\} + \beta\lambda^{\mathrm{B}}\left\{1 - \sum_{j=1}^{4} X_j^{\mathrm{B}}\right\}, \tag{9}$$

where λ^{A} and λ^{B} are introduced to maintain the normalization conditions, $\beta = \frac{1}{kT}$, T is the absolute temperature.

Thus, the self-consistent equation for four long-range order parameters, namely, M_{A}, Q_{A}, M_{B} and Q_{B} are therefore obtained by

$$\frac{\partial f}{\partial X_i^{\mathrm{A}}} = 0 \quad (i = 1,2,3,4) \quad \text{and} \quad \frac{\partial f}{\partial X_j^{\mathrm{B}}} = 0 \quad (j = 1,2,3,4). \tag{10}$$

Using (3), (9), and (10), the self-consistent equations are found to be

$$\begin{aligned}
M_{\mathrm{A}} &= \frac{3\mathrm{e}^{\frac{9}{4}\beta(KQ_{\mathrm{B}}-D)}\sinh\left[\frac{3}{2}\beta(JM_{\mathrm{B}}+H)\right] + \mathrm{e}^{\frac{1}{4}\beta(KQ_{\mathrm{B}}-D)}\sinh\left[\frac{1}{2}\beta(JM_{\mathrm{B}}+H)\right]}{2\mathrm{e}^{\frac{9}{4}\beta(KQ_{\mathrm{B}}-D)}\cosh\left[\frac{3}{2}\beta(JM_{\mathrm{B}}+H)\right] + 2\mathrm{e}^{\frac{1}{4}\beta(KQ_{\mathrm{B}}-D)}\cosh\left[\frac{1}{2}\beta(JM_{\mathrm{B}}+H)\right]}, \\
M_{\mathrm{B}} &= \frac{3\mathrm{e}^{\frac{9}{4}\beta(KQ_{\mathrm{A}}-D)}\sinh\left[\frac{3}{2}\beta(JM_{\mathrm{A}}+H)\right] + \mathrm{e}^{\frac{1}{4}\beta(KQ_{\mathrm{A}}-D)}\sinh\left[\frac{1}{2}\beta(JM_{\mathrm{A}}+H)\right]}{2\mathrm{e}^{\frac{9}{4}\beta(KQ_{\mathrm{A}}-D)}\cosh\left[\frac{3}{2}\beta(JM_{\mathrm{A}}+H)\right] + 2\mathrm{e}^{\frac{1}{4}\beta(KQ_{\mathrm{A}}-D)}\cosh\left[\frac{1}{2}\beta(JM_{\mathrm{A}}+H)\right]}, \\
Q_{\mathrm{A}} &= \frac{9\mathrm{e}^{\frac{9}{4}\beta(KQ_{\mathrm{B}}-D)}\cosh\left[\frac{3}{2}\beta(JM_{\mathrm{B}}+H)\right] + \mathrm{e}^{\frac{1}{4}\beta(KQ_{\mathrm{B}}-D)}\cosh\left[\frac{1}{2}\beta(JM_{\mathrm{B}}+H)\right]}{4\mathrm{e}^{\frac{9}{4}\beta(KQ_{\mathrm{B}}-D)}\cosh\left[\frac{3}{2}\beta(JM_{\mathrm{B}}+H)\right] + 4\mathrm{e}^{\frac{1}{4}\beta(KQ_{\mathrm{B}}-D)}\cosh\left[\frac{1}{2}\beta(JM_{\mathrm{B}}+H)\right]}, \\
Q_{\mathrm{B}} &= \frac{9\mathrm{e}^{\frac{9}{4}\beta(KQ_{\mathrm{A}}-D)}\cosh\left[\frac{3}{2}\beta(JM_{\mathrm{A}}+H)\right] + \mathrm{e}^{\frac{1}{4}\beta(KQ_{\mathrm{A}}-D)}\cosh\left[\frac{1}{2}\beta(JM_{\mathrm{A}}+H)\right]}{4\mathrm{e}^{\frac{9}{4}\beta(KQ_{\mathrm{A}}-D)}\cosh\left[\frac{3}{2}\beta(JM_{\mathrm{A}}+H)\right] + 4\mathrm{e}^{\frac{1}{4}\beta(KQ_{\mathrm{A}}-D)}\cosh\left[\frac{1}{2}\beta(JM_{\mathrm{A}}+H)\right]}.
\end{aligned} \tag{11}$$

We should mention that, since the behaviour of R_{A} and R_{B} is similar to M_{A} and M_{B}, we have not written R_{A} and R_{B} and investigated their behaviour, as many researchers have made. We are now able to examine the behaviour of the order parameters of the ferromagnetic spin-$\frac{3}{2}$ BEG model in an external magnetic field by solving the self-consistent equations, i. e. (11), numerically. In the following section, we shall examine the thermal variation of the systems.

It is worthwhile to mention that the values of these sublattice order parameters define five different phases with different symmetry as follows:

(i) Disordered phase (d): $M_{\mathrm{A}} = M_{\mathrm{B}} = 0$, $Q_{\mathrm{A}} = Q_{\mathrm{B}} \neq 0$.

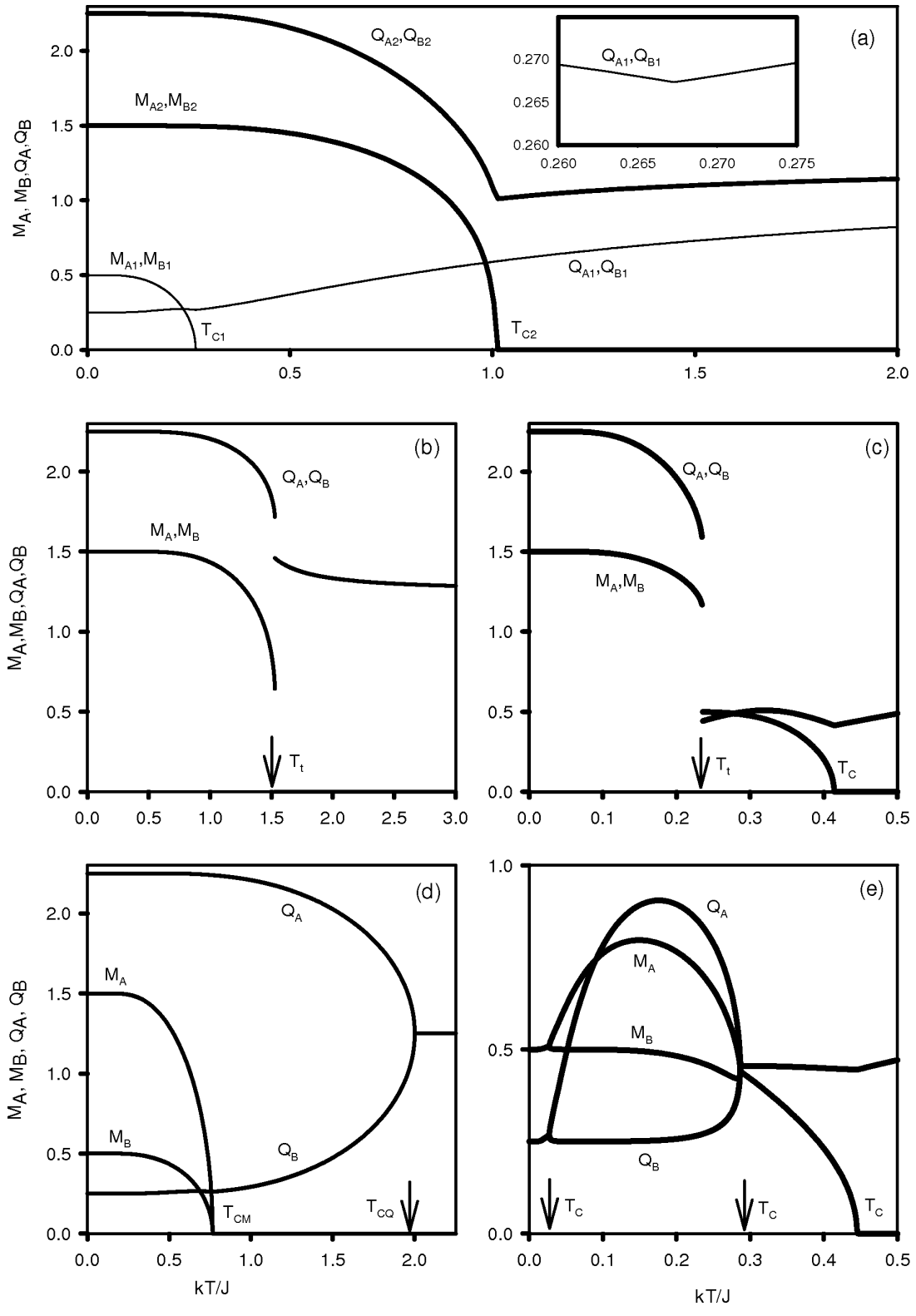
(a)
Q_{A2},Q_{B2}
M_{A2},M_{B2}
Q_{A1},Q_{B1}
M_{A1},M_{B1}
T_{C1}
T_{C2}
M_A, M_B, Q_A, Q_B
(b)
Q_A,Q_B
M_A,M_B
T_t
M_A,M_B,Q_A,Q_B
(c)
Q_A,Q_B
M_A,M_B
T_t
T_C
(d)
Q_A
M_A
M_B
Q_B
T_{CM}
T_{CQ}
M_A, M_B, Q_A, Q_B
kT/J
(e)
Q_A
M_A
M_B
Q_B
T_C
T_C
T_C
kT/J

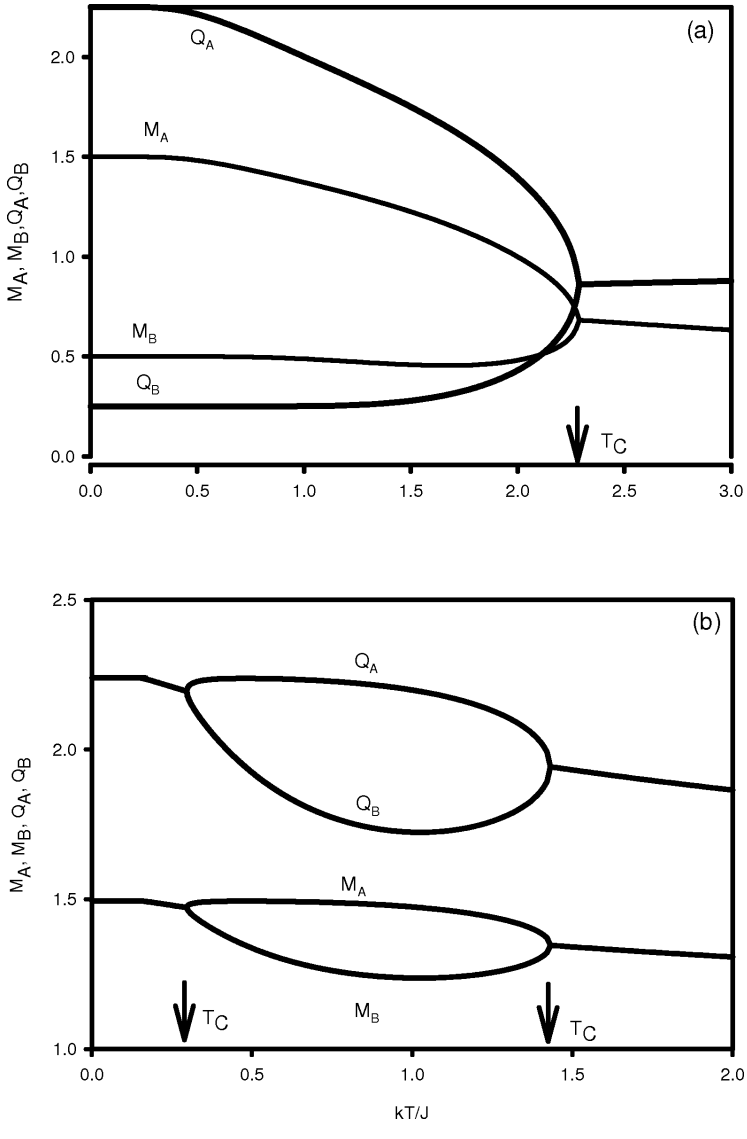

Fig. 2. Same as Fig. 1, but (a) $K/J = -3.0$, $D/J = 0.0$ and $H/J = 3.0$; (b) $K/J = -3.0$, $D/J = 0.0$ and $H/J = 12.75$.

(ii) Ferromagnetic-3/2 phase ($f_{3/2}$): $M_A = M_B = 3/2$, $Q_A \neq Q_B \neq 0$.

(iii) Ferromagnetic phase-1/2 ($f_{1/2}$): $M_A = M_B = 1/2$, $Q_A \neq Q_B \neq 0$.

(iv) Ferrimagnetic phase (i): $M_A \neq M_B \neq 0$, $Q_A \neq Q_B \neq 0$.

(v) Antiquadrupolar phase or staggered quadrupolar phase (a): $M_A = M_B = 0$ or $Q_A \neq Q_B \neq 0$.

3. Thermal Variations

In this section we shall study the temperature dependency of the order parameters in the absence and presence of an external magnetic field by solving the system of transcendental equations, namely the set of self-consistent equations, i. e. (11), numerically. These equations are solved by using the Newton-Raphson method and the thermal variations of M_A, M_B, Q_A and Q_B for several of coupling parameters, D/J, K/J and H/J. They are plotted in Figs. 1 and 2. In the figures, T_C and T_t, are the critical or the second-order phase transition temperatures and the first-order phase transition temperatures, respectively. T_{CM} and T_{CQ} represent the critical or the second-order phase transition temperatures for only the sublattice magnetizations and quadrupolar order parameters, respectively. First, we

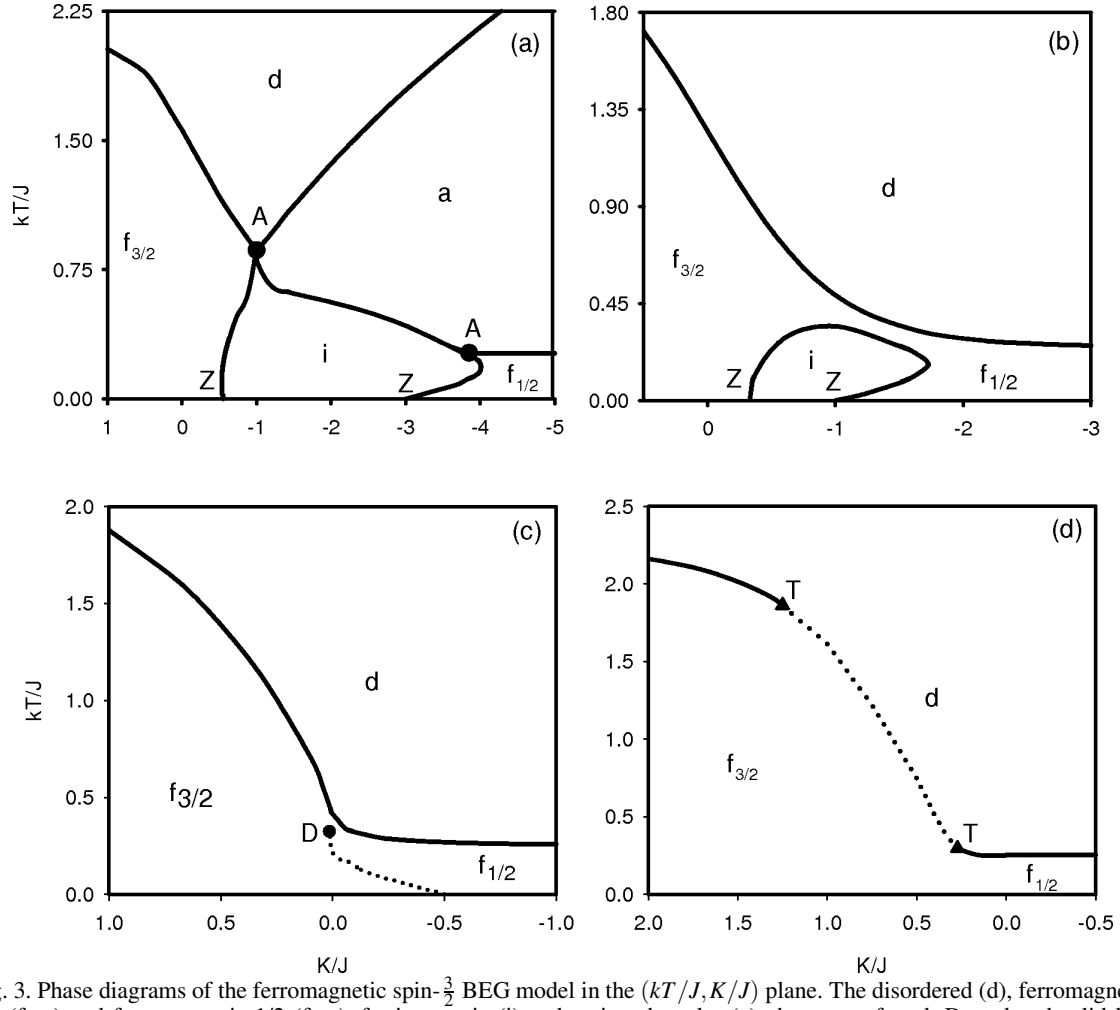

Fig. 3. Phase diagrams of the ferromagnetic spin-$\frac{3}{2}$ BEG model in the $(kT/J, K/J)$ plane. The disordered (d), ferromagnetic-3/2 ($f_{3/2}$) and ferromagnetic-1/2 ($f_{1/2}$), ferrimagnetic (i) and antiquadrupolar (a) phases are found. Dotted and solid lines indicate, respectively, first- and second-order phase transitions. The special points are the tricritical (T), multicritical (A), double critical (D) and zero-temperature critical point (Z). (a) $D/J = -0.5$; (b) $D/J = 0.0$; (c) $D/J = 0.5$; (d) $D/J = 1.0$.

will investigate the thermal variations of the sublattice magnetizations and quadrupolar order parameters in the absence of an external magnetic field. In this case, the behaviour of the temperature dependence of order parameters depends on K/J and D/J values, and following five main topological different types of behaviours are found by investigating these behaviours. They are plotted in Figure 1.

(a) *Type 1*: For $K/J = 0.25$ and $D/J = 0.5$, $M_A = M_B = 3/2$, $Q_A = Q_B = 2.25$ at zero temperature (thick solid lines) and for $K/J = -0.5$ and $D/J = 0.5$, $M_A = M_B = 1/2$, $Q_A = Q_B = 0.25$ at zero temperature (thin solid lines). For both lines, M_A and M_B decrease to zero continuously as the reduced temperature (kT/J) increases therefore the system exhibits a second-order phase transition, and the transition is from the ferromagnetic-3/2 phase ($f_{3/2}$) to the disordered (d) phase for the thick solid line and the ferromagnetic-1/2 phase ($f_{1/2}$) to the disordered (d) phase for the thin solid line. Q_A and Q_B make a cusp at T_{C1} and T_{C2}, as seen in Figure 1a.

(b) *Type 2*: For $K/J = 1.25$ and $D/J = 1.5$, $M_A = M_B = 3/2$ and $Q_A = Q_B = 2.25$ at zero temperature. The sublattice order parameters decrease to zero discontinuously as the reduced temperature increases; hence the system undergoes a first-order phase transition as seen in Figure 1b. The transition is also from the $f_{3/2}$ phase to the d phase.

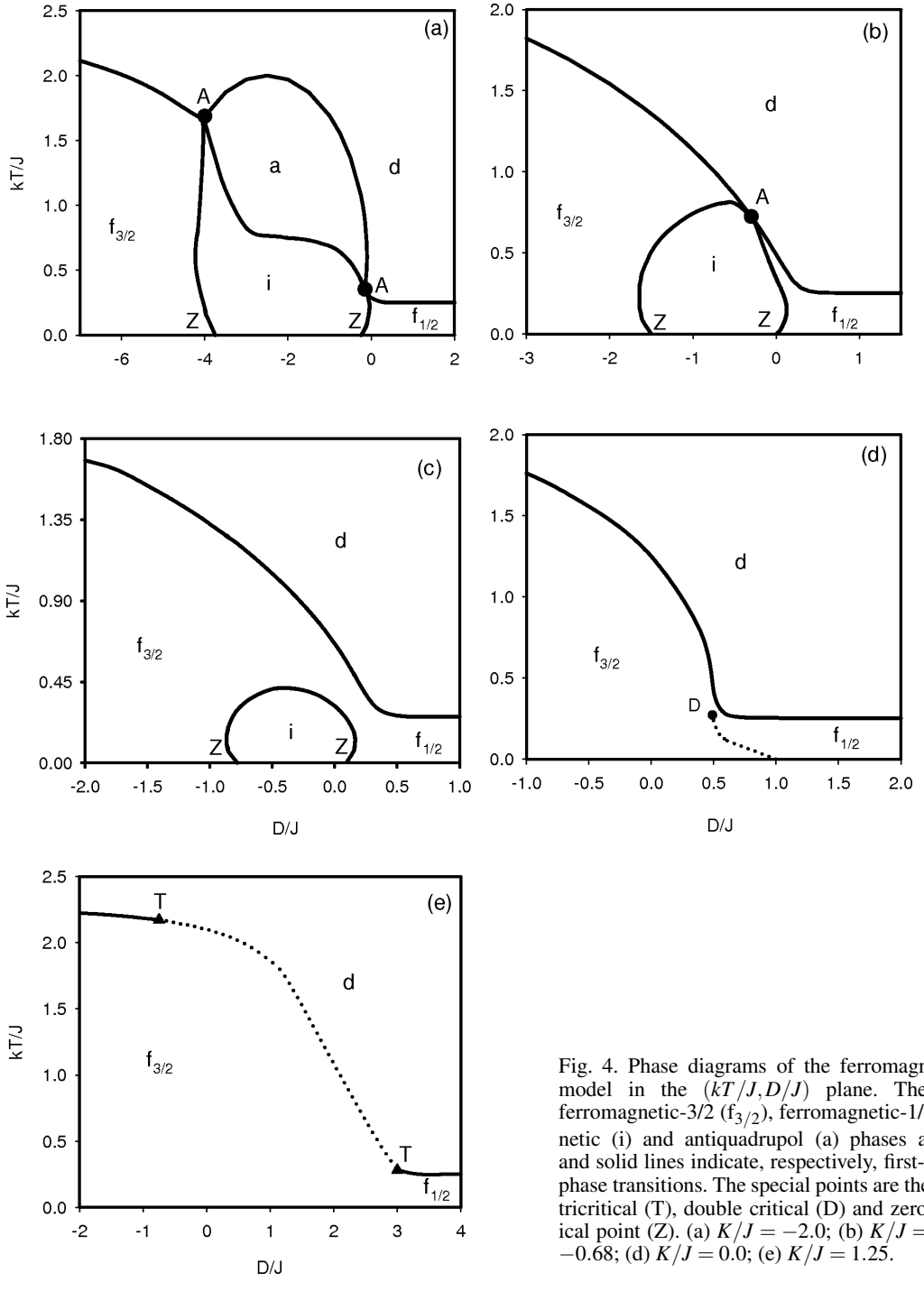

Fig. 4. Phase diagrams of the ferromagnetic spin-$\frac{3}{2}$ BEG model in the $(kT/J, D/J)$ plane. The disordered (d), ferromagnetic-3/2 ($f_{3/2}$), ferromagnetic-1/2 ($f_{1/2}$), ferrimagnetic (i) and antiquadrupol (a) phases are found. Dotted and solid lines indicate, respectively, first- and second-order phase transitions. The special points are the multicritical (A), tricritical (T), double critical (D) and zero-temperature critical point (Z). (a) $K/J = -2.0$; (b) $K/J = -1.0$; (c) $K/J = -0.68$; (d) $K/J = 0.0$; (e) $K/J = 1.25$.

(c) *Type 3*: For $K/J = -0.01$ and $D/J = 0.5$, $M_A = M_B = 3/2$ and $Q_A = Q_B = 2.25$ at zero temperature. The system undergoes two successive phase transitions, the first one is a first-order one from the $f_{3/2}$ phase to the $f_{1/2}$ phase and the second one is a second-order one, from the $f_{1/2}$ phase the d phase as seen in

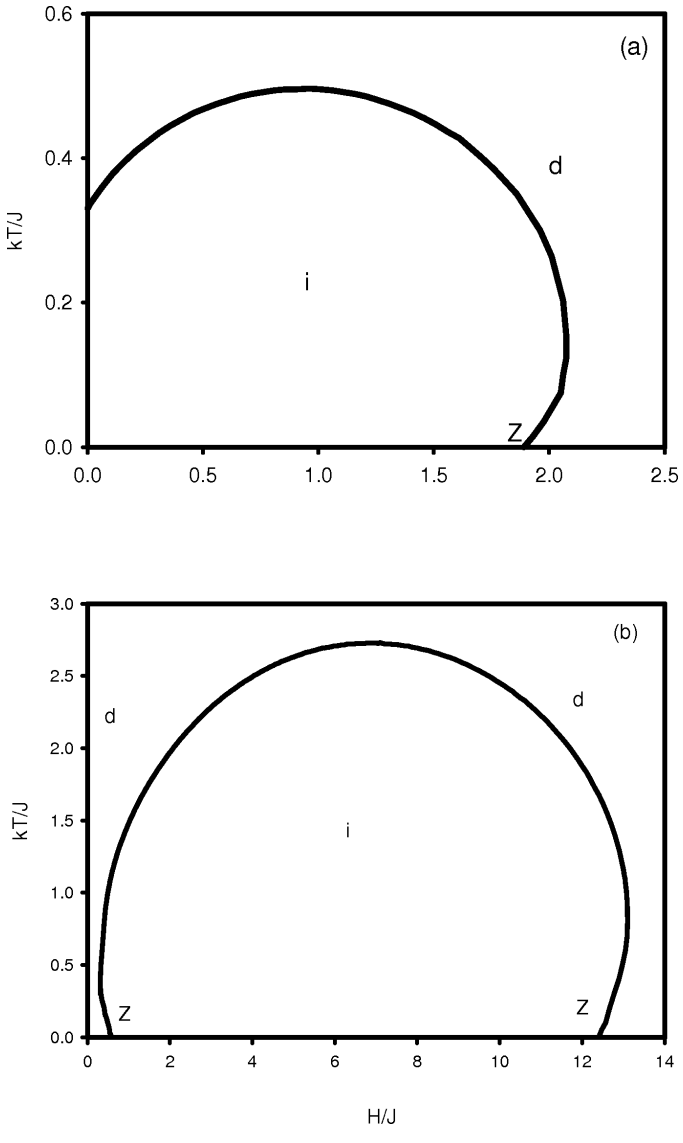

Fig. 5. Phase diagrams of the ferromagnetic spin-$\frac{3}{2}$ BEG model in the $(kT/J,H/J)$ plane. The solid line denotes the second-order phase transition line. The disorder (d), ferrimagnetic (i) phases are found. The special point is the zero-temperature critical point (Z). (a) $K/J = -0.75$ and $D/J = 0.0$; (b) $K/J = -3.0$ and $D/J = 0.0$.

Figure 1c. This fact is seen in the phase diagram of Fig. 3c explicitly. Compare Fig. 1c with Figure 3c.

(d) *Type 4*: For $K/J = -2.0$ and $D/J = -2.5$, $M_A = 3/2$, $M_B = 1/2$ and $Q_A = 2.25$, $Q_B = 0.25$ at zero temperature. The system undergoes two successive phase transitions, the first one is of second-order one from the i phase to the a phase, and the second one is also of second-order, from the a phase to the d phase as seen in Figure 1d. This fact is seen in the phase diagram of Fig. 4a explicitly. Compare Fig. 1d with Figure 4a.

(e) *Type 5*: For $K/J = -1.0$ and $D/J = 0.05$, $M_A = M_B = 1/2$ and $Q_A = Q_B = 0.25$ at zero temperature. In this type, the system undergoes three successive second-order phase transitions as seen in Figure 1e. The first two are second-order transitions, the first one is from the $f_{1/2}$ phase to the i phase and the second one is from the i phase to the $f_{1/2}$ phase; this implies that the system exhibits a reentrant behaviour. The third one implies that the transition is from the $f_{1/2}$ phase to the d phase. This fact is seen in the phase diagram of Fig. 4b explicitly. Compare Fig. 1e with Figure 4b.

On the other hand, Fig. 2 illustrates the temperature dependence of the sublattice order parameters in the presence of an external magnetic field, and the be-

haviour depends on D/J, K/J and H/J. The following two fundamental types of behaviour are found:

(a) *Type 1*: For $K/J = -3.0$, $D/J = 0.0$ and $H/J = 3.0$, $M_A = 3/2$, $M_B = 1/2$ and $Q_A = 2.25$, $Q_B = 0.25$ at zero temperature. The system undergoes a second-order phase transition from the i phase to the d phase, illustrated in Figure 2a. This fact is seen in the phase diagram of Fig. 5b explicitly. Compare Fig. 2a with Figure 5b.

(b) *Type 2*: For $K/J = -3.0$, $D/J = 0.0$ and $H/J = 12.75$, $M_A = M_B = 3/2$ and $Q_A = Q_B = 2.25$ at zero temperature. As the temperature increases, the sublattice order parameters undergo two successive second-order phase transitions at two different temperatures as seen in Figure 2b. This implies that the system exhibits a reentrant behaviour. This fact is seen explicitly in Figure 5b.

Finally we should mention that besides the stable solution order parameters metastable and unstable solution order parameters appear in the system. This classification is done by comparing the free energy values of these solutions with the lowest values of the free energy surfaces. The stable states or solutions correspond to the lowest minimum, metastable solutions correspond to a secondary or local minimum, and unstable solutions correspond to the local maxima (the peaks) or saddle points of the free energy surfaces. We have only considered the stable states or solutions of the order parameters.

4. Phase Diagrams

In this section, we present the phase diagram of the ferromagnetic spin-$\frac{3}{2}$ BEG model in the absence and the presence of an external magnetic field. The critical or second-order phase transition temperatures for the sublattice order parameters in the case of a second-order phase transition are calculated numerically, i. e., the investigation of the behaviour of the order parameters as functions of the temperature in which the sublattice order parameters become equal as the temperature is lowered and the temperature where the sublattice order parameters become equal is the critical or second-order phase transition temperature or the sublattice order parameters decrease to zero continuously as the reduced temperature increases; the temperature where $M_A = M_B = 0$ is the second-order phase transition temperature. Q_A and Q_B make a cusp at this temperature. On the other hand, the first-order phase transition temperatures for the sublattice order parameters are found by matching the values of the two branches of the free energy followed, while increasing and decreasing the temperature. The temperature at which the free energy values equal is the first-order phase transition temperature (T_t) for the sublattice order parameters.

The calculated phase diagrams are presented in Figures 3 – 6. In the phase diagrams, the solid line represents the second-order phase transition line, and the dotted line is the first-order phase transition line. A, T, D and Z are special points which denote the multicritical, tricritical, double critical and zero-temperature critical points, respectively. Figure 3 shows the phase diagram of the model in the absence of an external magnetic field in the $(kT/J, K/J)$ plane for various values of D/J. Four different diagram topologies have been found in this plane, the topology depending on D/J values.

(a) For $D/J = -0.5$, besides the disordered phase (d), the ferromagnetic-3/2 ($f_{3/2}$) and the ferromagnetic-1/2 ($f_{1/2}$), ferrimagnetic (i) and antiquadrupolar phase (a) also exist in the phase diagram of Figure 3a. All the phase boundaries among these phases are second-order lines. The phase diagrams also exhibit two multicritical (A), and two zero-temperature critical (Z) points. We should also mention that the system exhibits a reentrant behaviour, e. g., as the temperature is lowered, there are transitions from the d phase to the a phase, from the a phase to the i phase and from the i phase to the $f_{1/2}$ phase. This is a new phase diagram topology, which is either absent from previous approaches or has gone unnoticed.

(b) For $D/J = 0.0$, the phase diagram presents the d, $f_{3/2}$, $f_{1/2}$ and i phases, and it exhibits only two special Z points, illustrated in Figure 3b. The i phase lies at low temperatures, and the phase boundaries among three phases are all second-order lines. One should also notice a pronounced reentrance occurring in this diagram. A similar phase diagram has been obtained in the ferromagnetic spin-$\frac{3}{2}$ BEG model within the MFA [8], the EFT [9] and the CVMPA for the coordination number $q < 6$ [10], as well as the exact formulation of the model on the Bethe lattice by using the exact recursion equations [12, 13] for $q < 6$, but only differs in that the reentrant behaviour does not exist in these two works. However, the exactly similar phase diagram was obtained for $q > 6$ in [10] and [13].

(c) For $D/J = 0.5$, the phase diagram is similar to Fig. 1b, except for the i phase and as well as two zero-temperature critical points disappear as seen in Figure 1c. The phase boundary between the $f_{3/2}$ and

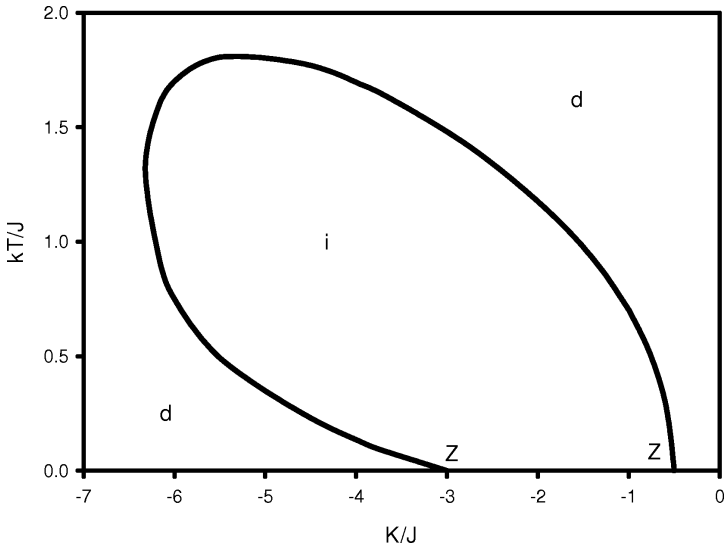

Fig. 6. Phase diagrams of the ferromagnetic spin-$\frac{3}{2}$ BEG model for $H/J \neq 0$ in the $(kT/J, K/J)$ plane. The solid line denotes the second-order phase transition line. The disordered (d) and ferrimagnetic (i) phases are found. $H/J = 1.0$ and $D/J = 0.0$.

the $f_{1/2}$ phase is a first-order line that starts from zero temperature and terminates a double critical (D) point, where two different critical systems coexist. This is also a new phase diagram topology in this plane, which is either absent from previous approaches or has gone unnoticed. We should also mention that a similar phase diagram, except for the first-order phase line, has been obtained in a ferromagnetic spin-$\frac{3}{2}$ BEG model within the CVMPA [10] and the exact formulation of the model on the Bethe lattice by using the exact recursion equations [12].

(d) For $D/J = 1.0$, the diagrams contain first-order and second-order phase transition lines as seen in Figure 3d. The phase boundary between the $f_{3/2}$ and d phase for very high values of the reduced temperatures (kT/J) and the boundary between the $f_{1/2}$ and d phases for very low values of kT/J are second-order phase lines. Between these very high and low values of kT/J, the first-order phase line occurs, and it separates the $f_{3/2}$ phase from the d phase. Therefore, two tricritical points exist in the phase diagram. This is also a new phase diagram topology, which is either absent from previous approaches or has gone unnoticed.

Figure 4 illustrates the phase diagram of the model in the absence of an external magnetic field in the $(kT/J, D/J)$ plane for various values of K/J. Study of the phase diagram in the $(kT/J, D/J)$ plane yields five typical situations depending on the value of K/J.

(a) For $K/J = -2.0$, in this phase diagram besides the disordered phase (d), the ferromagnetic-3/2 ($f_{3/2}$) and the ferromagnetic-1/2 ($f_{1/2}$), ferrimagnetic (i) and antiquadrupolar phase (a) also exist and all the phase boundaries among these phases are second-order lines as seen in Figure 4a. The phase diagrams also exhibit two multicritical (A) and two zero-temperature critical points (Z). We should also mention that the reentrance also occurs for the second-order phase transition line, which separates the i phase from the $f_{3/2}$ phase. A similar phase diagram topology has been obtained in the ferromagnetic spin-$\frac{3}{2}$ BEG model on the Bethe lattice by using the exact recursion equations by Ekiz et al. [12], except for the following differences: (1) the reentrant behaviour has not been observed for the second-order phase transition line which separates the i phase from the $f_{3/2}$ phase; (2) the phase boundary between the a and d phases is a first-order phase line.

(b) For $K/J = -1.0$, this phase diagram is similar to the phase diagram of Fig. 4a, except that the a phase disappears, hence only one multicritical point exist, presented in Figure 4b. This phase diagram agrees very well with the work of Ekiz et al. [12].

(c) For $K/J = -0.68$, this phase diagram is illustrated in Figure 4c. It agrees very well with previous works [11, 12], but differs from these previous works in that the reentrant behaviour does not occur for the second-order phase transition line which separates the i phase from the $f_{3/2}$ and $f_{1/2}$ phases.

(d) For $K/J = 0.0$, the topology of this phase diagram is very similar to the phase diagram of Fig. 3c, except for the one obtained in the $(kT/J, D/J)$ plane as seen in Figure 4d. This phase diagram agrees very

well with the works [8, 9, 12], except for the first-order phase transition line.

(e) For $K/J = 1.25$, the topology of this phase diagram is also very similar to the phase diagram of Fig. 3d, except for the one obtained in the $(kT/J, D/J)$ plane as seen in Figure 4e. Thus, the phase boundary between the $f_{3/2}$ and d phase for very high values of the reduced temperatures (kT/J) and the boundary between the $f_{1/2}$ and d phases for very low values kT/J are second-order phase lines. Between these very high and low values of kT/J, the first-order phase line occurs and it separates the $f_{3/2}$ phase from the d phase. Therefore, two tricritical points exist in the phase diagram. This is also a new phase diagram topology, which is either absent from previous approaches or has gone unnoticed.

We have also presented the phase diagrams of the model in the presence of an external magnetic field in the $(kT/J, H/J)$ and $(kT/J, K/J)$ planes. We have two different phase diagram topologies in the $(kT/J, H/J)$ plane, presented in Figs. 5a and b, in which one of them, Fig. 5a shows a similar phase diagram topology as recently obtained by Ekiz [13] for $q > 6$, q is the coordination number. The other phase diagram, Fig. 5b, is a new phase diagram topology, which is either absent from previous approach, namely [13] or has gone unnoticed. Figure 6 presents the phase diagram for $D/J = 0.0$ and $H/J = 1.0$ in the $(kT/J, K/J)$ plane. The topology of this phase diagram is very similar to the phase diagram of Fig. 5b, except for the one obtained in $(kT/J, K/J)$ plane seen in Figure 6. This phase diagram also agrees very well with the recent work for $q > 6$ [13]. Moreover, these three phase diagrams exhibit a reentrant behaviour.

5. Summary and Discussion

In this work, first we have investigated the thermal variations of the ferromagnetic spin-$\frac{3}{2}$ BEG model in the presence and absence of an external magnetic field by using the LACVM in detail. Figure 1 shows the behaviours of the temperature dependence of the sublattice order parameters in the absence of an external magnetic field. These behaviours depend on K, D and $J > 0$ values, and five main different topological types are found by investigating these behaviours. Figure 2 illustrates the thermal variations of the sublattice order parameters for the presence of an external magnetic field, in which these behaviours depend on K, D, H and $J > 0$ values, and two different topologies are found by investigating these behaviours. Then, we have presented the global phase diagrams of the system in the $(kT/J, K/J)$ and $(kT/J, D/J)$ planes for the absence of an external magnetic field. For the $(kT/J, K/J)$ plane, we found that the behaviour of the system strongly depends on the values of D/J, and four different phase diagram topologies were found as seen in Figure 3. In this case we have obtained three new phase diagram topologies with careful and painstaking calculations that were not obtained in previous works [8 – 13], which are either absent from previous approaches or have gone unnoticed. For the $(kT/J, D/J)$ plane, we found that the behaviour of the system strongly depends on the values of K/J, and five different phase diagram topologies were found, illustrated in Figure 4. In this case, we have also obtained only one new phase diagram topology by careful calculations, that was not obtained in previous works [8 – 13], which is either absent from previous approaches or has gone unnoticed. We have also presented the phase diagram of the model in the presence of an external magnetic field in the $(kT/J, H/J)$ and $(kT/J, K/J)$ planes. We have two different phase diagram topologies in the $(kT/J, H/J)$ plane, in which one is a similar phase diagram topology as obtained in the work of Ekiz [13] recently for $q > 6$, q is the coordination number and the other is a new phase diagram topology, which is either absent in [13] or has gone unnoticed. Only one phase diagram topology in the $(kT/J, K/J)$ plane is found, and it agrees very well with the recent work for $q > 6$ [13].

We should also mention that, although we have obtained five new phase diagram topologies, we could not find one of the phase diagram topologies which was obtained in the $(kT/J, D/J)$ plane within an approximate renormalization-group approach of the Migdal-Kadanoff type [11] and an exact formulation of the model on the Bethe lattice [12]. Moreover, we could not obtain two topologies of phase diagrams in the $(kT/J, K/J)$ plane, which were presented in [12]. These are the shortcoming of this simple, but important and effective method. Hence, we have concluded that the mean-field type calculation, in spite of its simplicity and limitations such as the correlation of spin fluctuations have not been considered, is still an adequate starting point, in which within this theoretical framework it is easy to determine the complete phase diagrams. It also predicts the existence of multicritical points in simple, such as spin-$\frac{1}{2}$ Ising model [18]

and complex, e. g., the spin-1 Ising [17, 20, 21], and the spin-$\frac{3}{2}$ Ising system [15, 16]. Finally, we should also point out the following fact. It is well known that mean-field-like approximations as the one we used in the present analysis may even be qualitatively wrong for low-dimensional systems. Therefore, there is a possibility that some of the phase lines and multicritical points seen in the phase diagrams are artifacts of the approximation. Hence, it would be worthwhile to further study it with more sophisticated techniques, such as renormalization-group calculations or Monte Carlo simulations.

Acknowledgements

This research was supported by the Research Found of Erciyes University, grant number FBT-05-03.

[1] J. Sivardière and M. Blume, Phys. Rev. B **5**, 1126 (1972).
[2] A. H. Cooke, D. M. Martin, and M. R. Wells, Solid State Commun. **9**, 519 (1971); A. H. Cooke, D. M. Martin, and M. R. Wells, J. Phys. (Paris) Colloq. **32**, C1-488 (1971).
[3] S. Krinsky and D. Mukamel, Phys. Rev. B **11**, 399 (1975).
[4] A. Bakchich, A. Bassir, and A. Benyuossef, Physica A **195**, 188 (1993).
[5] T. Kaneyoshi and M. Jaščur, Phys. Lett. A **177**, 172 (1993).
[6] N. Tsushima, Y. Honda, and T. Horiguchi, J. Phys. Soc. Jpn. **66**, 3053 (1997).
[7] E. Albayrak and M. Keskin, J. Magn. Magn. Mater. **241**, 249 (2002).
[8] F. C. Sâ Barreto and O. F. De Alcantara Bonfim, Physica A **172**, 378 (1991).
[9] A. Bakkali, M. Kerouad, and M. Saber, Physica A **229**, 563 (1996).
[10] J. W. Tucker, J. Magn. Magn. Mater. **214**, 121 (2000).
[11] A. Backhich and M. El Bouziani, J. Phys.: Condens. Matter **13**, 249 (2001).
[12] C. Ekiz, E. Albayrak, and M. Keskin, J. Magn. Magn. Mater. **256**, 311 (2003).
[13] C. Ekiz, Phys. Status Solidi (b) **241**, 1324 (2004).
[14] R. Kikuchi, Phys. Rev. **81**, 988 (1951); R. Kikuchi, Crystals Statistics, Hughes Research Lab., Malibu, CA 1979 (unpublished); H. Şişman and M. Keskin, Tr. J. Phys. **14**, 88 (1990).
[15] M. Keskin, M. Ali Pınar, A. Erdinç, and O. Canko, Phys. Lett. A **353**, 116 (2006) and references therein.
[16] M. Keskin, M. Ali Pınar, A. Erdinç, and O. Canko, Physica A **364**, 263 (2006) and references therein.
[17] A. Erdinç, O. Canko, and M. Keskin, J. Magn. Magn. Mater. **301**, 6 (2006).
[18] G. Refael, S. Kehrein, and D. S. Fisher, Phys. Rev. B **66**, 060402 (2002).
[19] A. Saguia, B. Boechat, and M. A. Continentino, Phys. Rev. B **68**, 020403(R) (2003).
[20] W. Hoston and A. N. Berker, Phys. Rev. Lett. **67**, 1027 (1991).
[21] C. Ekiz and M. Keskin, Phys. Rev. B **66**, 54105 (2002).